Study on the adsorption of polystyrene microplastics by three-dimensional reduced graphene oxide

Fang Yuan, Lingzhi Yue, Han Zhao and Huifang Wu

ABSTRACT

In this paper, a study on the removal of imitated polystyrene (PS) microplastics in water was carried out based on the adsorption capacity of three-dimensional reduced graphene oxide (3D RGO). Scanning electron microscopy and X-ray diffractometry characterization showed that the freeze-dried 3D RGO formed a distinct porous spatial structure. Different experimental parameters, such as pH, ion concentration (C_0), contact time (t), and temperature (T), were studied to investigate the PS microplastic adsorption performance of 3D RGO. The adsorption mechanism was mainly attributed to the strong π–π interaction between the carbon ring of 3D RGO and the benzene ring of PS microplastics. Sorption kinetic and isothermal data were obtained by the well-fitted Langmuir adsorption isotherm model and pseudo-second-order kinetic model. Furthermore, the result of thermodynamic analysis showed that the adsorption of PS microplastics was a spontaneous endothermic process. Under the optimal conditions of pH = 6, C_0 = 600 mg/L, t = 120 min, and T = 26 °C, the maximum adsorption capacity of the prepared 3D RGO on PS microplastics was 617.28 mg/g. Furthermore, this method exhibited good feasibility in tap water and lake water.

Key words | adsorption, graphene, microplastics, polystyrene, porous structure

Fang Yuan (corresponding author)
Lingzhi Yue
Han Zhao
Huifang Wu
Department of Municipal Engineering,
College of Urban Construction,
Nanjing Tech University,
Nanjing 211816,
China
E-mail: *yuanf@njtech.edu.cn*

HIGHLIGHTS

- We used three-dimensional reduced graphene oxide to complete the adsorption of polystyrene microplastics in water.
- The maximum adsorption capacity of three-dimensional reduced graphene oxide for polystyrene microplastics was 617.28 mg/g, which was affected by pH, ion concentration, adsorption time, initial concentration and temperature.
- The adsorption mechanism was investigated, which was mainly attributed to the strong π–π force with the help of electrostatic attraction and physical retention.
- Langmuir adsorption isotherm model and pseudo-second-order kinetic model were well-fitted with experimental data, which indicated that the adsorption was chemical adsorption.
- The feasibility of this method in tap water and micro-polluted water was proved.

INTRODUCTION

Plastic wastes exist in various forms in the natural environment. These wastes are continuously cracked into small-sized particles or fragments under the action of physical degradation, biodegradation, and photodegradation (Cole *et al.* 2011; Hidalgo–Ruz *et al.* 2012; Auta *et al.* 2017). Microplastics are usually defined as plastic fragments, films, or particles with size less than 5 mm. Microplastics are currently proliferating in water, sediment, soil, and other media because of their chemical stability and slow degradation process compared with large plastics (Wu *et al.* 2017). They are easily eaten by plankton and fish, and then transferred and enriched in food chains and webs (Browne

doi: 10.2166/wst.2020.269

et al. 2008; Farrell et al. 2013). Finally, microplastics may even enter into the human body (Paul–Pont et al. 2016; Pellini et al. 2018). Microplastics are ideal carriers of many hydrophobic organic pollutants and heavy metals because of their small size, large specific surface area, and strong hydrophobicity (Shim & Thomposon 2015). Microplastics are currently of great public concern given their ubiquitous presence and persistence in the natural environment (Cózar et al. 2014).

However, at present, domestic and international studies on the treatment of microplastics are still at their primary stage. Large plastics are usually removed from the water by traditional means of bleaching. However, these methods are no longer applicable for microplastics due to their small size. Murphy et al. (2016) found that although 98.41% of plastics were removed through wastewater treatment, 65 million microplastic particles in the effluent still existed per day. Orb Media, a nonprofit news organization, reported that 159 drinking water samples from five continents were tested, and 83% of them were contaminated by tiny pieces of plastic debris (Peng et al. 2017). Wardrop et al. (2016) proved that the removal rate of plastic particles larger than 10 mm can reach 90% using ordinary wastewater treatment processes, but a large number of small plastic particles still enter the natural water body through drainage.

Therefore, some scholars have begun to study effective methods and technologies for the treatment of microplastics. Some scholars filter and collect microplastics in water through membrane devices prior to disposal. This approach draws lessons from some measures of algae bloom control. Ma et al. (2019) studied the removal behavior of polyethylene microplastics in flocculation and ultrafiltration processes. They found that the traditional flocculation process and flocculants cannot easily remove polyethylene microplastics, and the ultrafiltration process could remove polyethylene microplastics smaller than the pore size of a membrane. However, problems, such as high cost and membrane fouling, are still found in the process of removing microplastics from water by using membrane devices. Carr et al. (2016) studied seven tertiary sewage treatment plants and one secondary sewage treatment plant in southern California and simulated the distribution of microplastics in sewage in a laboratory. The results showed that the tertiary treatment could remove most of the microplastics. However, the secondary treatment could not effectively remove most of the microplastics. Magnusson & Fredrik (2014) studied microplastics in a Swedish sewage treatment plant in 2014. The results showed that the influent concentration was 3.2 million per hour, and the removal rate of the sewage treatment plant reached 99%. However, due to the huge throughput per day, a large amount of small-sized plastics still flow out. Therefore, high-efficiency and cost-effective methods are urgently needed. Among various methods, adsorption is widely used in wastewater treatment. Adsorption is usually used as an advanced and terminal treatment for residual small molecular pollutants in water. Compared with other methods, adsorption has the advantages of convenient operation, high purification rate, low energy consumption, and low cost (Akhtar et al. 2015). This approach is recognized as an important technology for wastewater treatment. Therefore, studying the removal of microplastics in water by adsorption is of practical value.

Some new materials, such as carbon nanotubes (CNTs) (Fattahi et al. 2015), titanium dioxide (Shojaie et al. 2018), and graphene, have been developed and utilized due to the wide application of adsorption methods. Graphene, as a type of new adsorbent materials, has attracted much attention in different fields. Compared with the traditional adsorption materials, such as activated carbon (Altmann et al. 2016), zeolite molecular sieve (Ge et al. 2014), and activated alumina (Tajizadegan et al. 2016), graphene has the advantages of large specific surface area, rich oxygen functional groups, and strong modifiability and adsorption capacity. Compared with other highly effective adsorption materials, such as CNTs, graphene has the advantages of simple preparation process and low price. Therefore, graphene and its derivatives have been widely used as adsorbents in the treatment of water pollutants. Jin et al. (2015) studied the adsorption capacity of magnetically reduced graphene oxide (RGO) on 4-nonylphenol and bisphenol A (BPA). The results showed that the adsorption capacity of the magnetically RGO on two organic pollutants was significantly higher than that of the activated carbon at pH = 6.5. Yang et al. (2010) found that the adsorption effect of graphene oxide on Cu^{2+} in water was almost 10 times that of activated carbon. Xu et al. (2012) studied the adsorption capacity of graphene on BPA in aqueous solution under different conditions. The results showed that the adsorption capacity of graphene on BPA is the highest among carbon adsorption materials.

However, a two-dimensional (2D) graphene can easily agglomerate in water due to the strong π–π stacking interaction between sheets, thereby decreasing its adsorption capacity. The 2D graphene can be assembled into a three-dimensional (3D) structure by self-assembly method, hydrothermal method (Kazemeini et al. 2016; Payan et al. 2018), and freeze-drying method. The 3D structure can not only effectively prevent the agglomeration of the graphene

sheets, but also facilitate the diffusion and adsorption of pollutants (Nardecchia *et al.* 2013; Shen *et al.* 2015). Also, the 3D structure can facilitate the solid–liquid separation after adsorption. Vadahanambi *et al.* (2013) found that the adsorption capacity of 3D graphene on arsenic in water is twice that of 2D graphene. Therefore, 3D graphene has a broader application prospect in the treatment of pollutant in water than 2D graphene.

In the present study, researchers use 3D RGO as adsorbent to remove this microscaled polystyrene (PS) microplastic. To the best of the researchers' knowledge, no related reports have been published thus far. Among various plastic pollution, PS microplastic pollution is particularly widespread. This type of plastic can inhibit the incubation and development of some aquatic organisms or disturb their energy absorption and metabolism, and then affect their breeding and offspring health. Different adsorption conditions were set to study the adsorption effect of 3D RGO on PS microplastics under different factors. The adsorption mechanism of 3D RGO for PS microplastics and the energy changes in the process of adsorption were obtained on the basis of the results of adsorption isotherms, adsorption kinetics, and thermodynamic analysis.

MATERIALS AND METHODS

Materials

Natural graphite, concentrated sulfuric acid (H_2SO_4, 98%), potassium permanganate ($KMnO_4$), hydrogen peroxide (H_2O_2, 30%), hydrochloric acid (HCl, 37%), sodium hydroxide (NaOH), and absolute ethanol (C_2H_6O) were purchased from Shengjianquan Chemical Glass Instrument Co., Ltd (Nanjing, China). Monodisperse PS microspheres (5 μm, white emulsion) were purchased from BaseLine Chrom Tech Research Center (Tianjin, China). The surface of the PS microspheres is smooth and has strong hydrophobicity. Ethanol, which reduces surface tension, was added and ultrasound was used to help in the dispersion.

Preparation of 3D RGO

Preparation of graphene oxide

Graphene oxide (GO) was prepared by the modified Hummers method (Marcano *et al.* 2010). Graphite powder (1 g) was thoroughly mixed with H_2SO_4 (23 mL, 98%) in an ice water bath. $KMnO_4$ (3 g) was slowly added (0.3 g/min), and the mixture was stirred continuously for 30 minutes until completely dissolved. Then, the mixture was allowed to stand for 48 h. After 48 h, the reaction was completed with the addition of distilled water (186 mL) and H_2O_2 (10 mL, 30%). The solution was maintained under constant stirring until the color of the solution changed to bright yellow. After the solution was cooled, it was centrifuged (TDL-400, Changzhou Youlian Instrument Co., Ltd, China) at 2,000 r/min for 15 minutes each time. The precipitate was retained and washed several times with HCl (5%) and distilled water until the supernatant was near neutral (pH = 5.0–6.0). The supernatant was decanted to obtain the GO dispersion.

Preparation of 3D RGO

RGO was prepared by the hydrothermal method (Marcano *et al.* 2010). The GO solution (3.5 mg/mL) was prepared by distilled water. Then, it was well dispersed by sonication (ultrasonic cleaner KQ-400DE, Shanghai Wanning Precision Scientific Instrument Co., Ltd, China) at room temperature for 15 minutes. The pH of the prepared GO solution (10 mL) was adjusted to pH = 8 with NaOH (1 mol/L). The solution was made up to 25 mL with distilled water and mixed well. Then, the mixture was transferred to polytetrafluoroethylene hydrothermal reactors and placed in an oven (DHG-9070A, Shanghai Yiheng Scientific Instrument Co., Ltd, China) at 180 °C. After 9 h, the reduction process was completed. The reactors were removed from the oven and allowed to cool at room temperature. Finally, the product was freeze-dried (vacuum freeze drier CTFD-12P, Qingdao Yonghe Chuangxin Electronic Technology Co., Ltd, China) to obtain a fluffy 3D RGO.

Characterization of 3D RGO

The surface morphology of 3D RGO was observed by scanning electron microscopy (SEM, JSM-6510, USA), and the chemical compositions were analyzed by X-ray diffractometry (XRD, Rigaku, Japan).

Standard curve of microplastic solution

The original solution of PS microspheres (250 mg/mL) was dispersed by ultrasound for 15 minutes to ensure that the microsphere was uniformly dispersed in the solution. The microplastic solution was diluted by the original solution of PS microspheres. A certain amount of original solution

was diluted by adding a certain amount of ethanol and distilled water (1:1). A series of microplastic solutions with concentrations of 0.1, 0.2, 0.3, 0.4, 0.5, 0.6, 0.7, and 0.8 g/L was prepared. The prepared solution (250 mg/mL) was dispersed by ultrasound for 15 minutes to ensure that the microsphere was uniformly dispersed in the solution. A full wavelength scan (ultraviolet–visible spectrophotometer, T6 new century, Beijing General Analysis General Instrument Co., Ltd, China) of the uniformly dispersed microplastic solution was carried out to determine the maximum absorbance wavelength of the microplastic solution at 720 nm. The absorbance of solutions at 720 nm at different concentrations was measured, and a standard curve was established to obtain the functional relationship between the concentration of microplastic solution and the absorbance.

Adsorption studies

A certain amount of original solution was diluted by adding a certain amount of ethanol and distilled water (1:1). The pH of the solution was adjusted with HCl (1 mol/L) or NaOH (1 mol/L). Finally, the volume was adjusted to obtain a concentration of 0.6 g/L of a microplastic solution using ethanol and distilled water (1:1). The prepared solution (0.6 g/L) was dispersed by ultrasound for 15 minutes to ensure that the microsphere was uniformly dispersed in the solution. An amount of 1.5 mg of the 3D RGO absorbents was added to 2 mL of the prepared solution (0.6 g/L). The mixture was placed in a water-bathing constant-temperature vibrator (SHA-C, Changzhou Guohua Electric Co., Ltd, China) and shaken for 2 hours at a speed of 160 r/min at 26 °C. After adsorption, the mixture was allowed to stand for 30 min to completely precipitate the adsorbent at the bottom and stratify with the solution to be measured. The supernatant was collected, and the absorbance value of the supernatant at 720 nm was recorded. The concentration of residual microplastic solution was calculated by the standard curve. The adsorption capacity (Q_e) of 3D RGO and the removal efficiency (R) of microspheres were calculated using the following equations:

$$Q_e = \frac{(C_0 - C_e)V}{m} \quad (1)$$

$$R = \frac{C_0 - C_e}{C_0} \times 100\% \quad (2)$$

where C_0 (mg/L) is the initial concentration, C_e (mg/L) is the concentration at the equilibrium of adsorption, V (L) is the volume of the solution, and m (g) is the quantity of the adsorbent.

Adsorption studies in actual water samples

The distilled water used in the experiment was exchanged for different actual water samples for adsorption experiments. The actual water samples are tap water and micropolluted water from a campus lake. The water quality indexes of the tap water are as follows: pH = 7.12 and dissolved oxygen (DO) = 3.5 mg/L. The water quality indexes of the micropolluted water are as follows: pH = 7.6, DO = 5.1 mg/L, turbidity = 15.42 NTU, chemical oxygen demand = 8.12 mg/L, NH_4^+-N = 2.83 mg/L, and total phosphorus = 0.98 mg/L. Prior to the experiment, the micropolluted water was pretreated by precipitation and filtration to obtain clear and transparent water. When the adsorption experiment was carried out in the actual water sample, the pH in the water was not adjusted with HCl or NaOH. The adsorption experiment was carried out in accordance with the procedure described under the following optimal conditions: $C_0 = 600$ mg/L, $t = 120$ min, and $T = 26$ °C.

RESULTS AND DISCUSSION

Characterization of 3D RGO

The surface morphology of 3D RGO was analyzed by SEM images, as shown in Figure S1(a)–(d) (Supplementary material). Figure S1(a) shows that the freeze-dried RGO has a fluffy appearance with a large number of pore structures on the surface. The internal pore structures of the RGO are connected to one another to form a 3D structure. After 1,000 times magnification (Figure S1(b) and S1(c)), the sheet of 3D RGO is evidently curly and gauzy, indicating that the peeling degree of 3D RGO is high. The surface of the sheet is rugged, and the size of the pores formed by the wrinkles and defects ranges from 10 to several micrometers. RGO forms a loose porous 3D structure, which avoids the disadvantage of easy coagulation of 2D planar structures. The 3D structure increases the specific surface areas and active sites of 3D RGO.

Figure S1(d) shows the result of energy spectrum analysis of 3D RGO. The weight ratio of carbon and oxygen in 3D RGO is approximately 76.98% and 18.77%, respectively, and the atomic ratio of carbon and oxygen in 3D RGO is approximately 81.96% and 15.98%, respectively. This finding indicates that most oxygen-containing groups in 3D

RGO are removed. The residual oxygen-containing groups increase the surface activity of 3D RGO and add new active sites for 3D RGO.

The XRD patterns of 3D RGO are presented in Figure S2 (Supplementary material). Natural graphite showed a strong peak at 26.5°, and GO showed a strong peak at approximately 10°; these peaks were associated to (002) and (001) planes, respectively, (Jeong *et al.* 2008; Zhou *et al.* 2009) and were narrow and sharp. The 3D RGO after thermal reduction exhibited a broad peak centered around 25° in the graphite region. The Bragg equation is as follows:

$$d = \frac{n\lambda}{2\sin\theta} \tag{3}$$

where d is the distance between the crystal planes, θ is the angle between the incident X-ray and the corresponding crystal plane, λ is the wavelength of the X-ray, and n is the number of diffraction orders. The interlayer distance of 3D RGO (0.36 nm) is larger than that of the natural graphite (0.34 nm) and GO (0.14 nm). This result may be the effect of the residual oxygen-containing functional groups in the 3D RGO. Thus, the crystal structure of the graphite cannot be completely repaired. As a result, stacking and agglomeration of the sheets are avoided. Thus, 3D RGO has a relatively large specific surface area and many active adsorption sites.

Effect of different factors on adsorption

In the preliminary study of the adsorption of microplastics, absorbance was used to represent the concentration of microplastic solution. The linear plot of the absorbance of the standard solution versus the concentration of the standard solution is presented in Figure S3 (Supplementary material). Figure S3 shows that the concentration of standard solution is linearly correlated with its absorbance at 720 nm. The formula is as follows:

$$y = 1.447x + 0.02564 \tag{4}$$

where y is the absorbance of the solution at 720 nm; x (g/L) is the concentration of standard solution. The correlation coefficient R^2 of linear fitting is 0.999, which indicates that the degree of linear fitting is perfect.

Initial pH

The pH of the solution was adjusted to 2, 4, 6, 7, 8, and 10 with HCl or NaOH (1 mol/L) to test the adsorption effect of 3D RGO on microplastics. Other experimental conditions were set according to the conditions described in the 'Adsorption studies' section.

As shown in Figure 1, with the increase in the initial pH value, the removal efficiency of microplastics and the adsorption capacity of the 3D RGO increased initially when pH increased from 2 to 6 and then decreased when pH increased from 6 to 10. At pH = 6, the removal efficiency of PS microplastics and the adsorption capacity of the 3D RGO reached the highest at 66.63% and 522.06 mg/g, respectively. After the GO was thermally reduced, most oxygen-containing functional groups were removed except for a small portion of residual oxygen-containing functional groups, such as carboxyl groups and hydroxyl groups (Huang *et al.* 2014). Under acidic conditions, the residual carboxyl group on 3D RGO exists in the form of $COOH_2^+$ due to the large amount of H^+, resulting in the positive charge on the surface of 3D RGO. With the increase in the initial pH value, the residual carboxyl group on 3D RGO exists in the form of COO^- due to the large amount of OH^-, resulting in the negative charge on the surface of 3D RGO. The changes in the surface of 3D RGO were further confirmed by zeta potential analysis, as shown in Figure 2. Compared with 3D graphene, the isoelectric point of PS microplastics was acidic, which may be related to $-SO_4^-$ on the surface of the microspheres. At the same time, with the increase in pH value, the zeta potential of PS microplastics appeared to plateau. This finding showed that, in a certain pH range, the microspheres had good dispersion and stability.

Figure 2 shows that 3D RGO was positively charged at pH = 2, which repulsed the positively charged PS

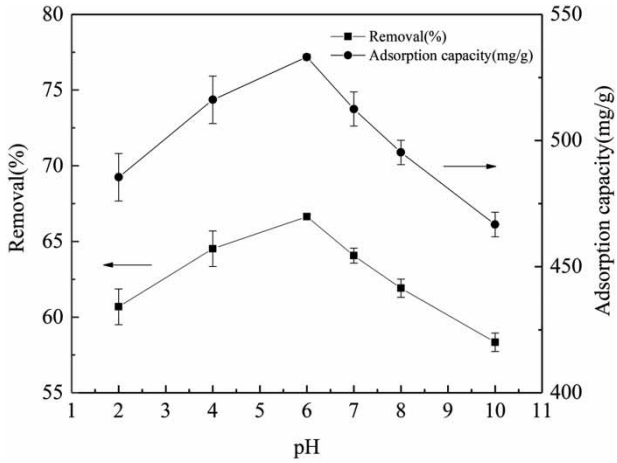

Figure 1 | Effect of different initial pH values on the adsorption of microplastics on 3D RGO.

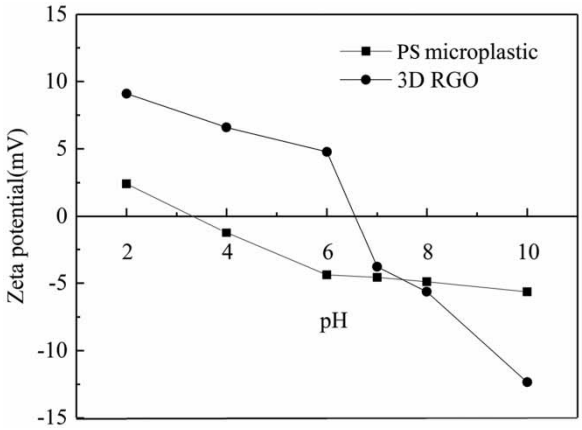

Figure 2 | Zeta potentials of 3D RGO and PS microplastics in different pH values.

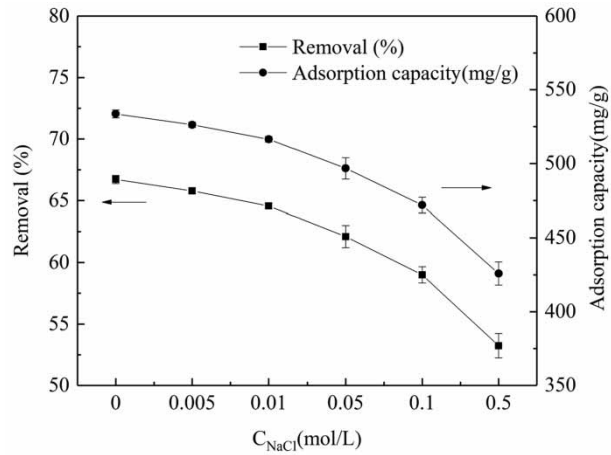

Figure 3 | Effect of different ion concentrations on the adsorption of PS microplastics on 3D RGO.

microplastics, resulting in the limited removal efficiency of microplastics and adsorption capacity of 3D RGO. At pH = 4, PS microplastics were slightly negatively charged, resulting in the promotion of the adsorption capacity of 3D RGO, which was positively charged due to the electrostatic attraction. At pH = 6, with the increase in the negative charges on the surface of PS microplastics, the electrostatic attraction between PS microplastics and 3D RGO increased, resulting in the highest removal efficiency of PS microplastics and the adsorption capacity of the 3D RGO. With increasing pH to >7, the PS microplastic and 3D RGO were negatively charged. Thus, the removal efficiency of PS microplastics and the adsorption capacity of the 3D RGO decreased.

Despite the electrostatic repulsion between 3D RGO and PS microplastics in acid and alkaline environments, the removal efficiency of 3D RGO for PS microplastics is still higher than 55%, and the difference between the highest and the lowest adsorption rate is less than 10%. This finding indicates that the effect of different initial pH values on the adsorption of PS microplastics on 3D RGO is insignificant. This result may expand the range of the application of this method.

Ion concentrations

The concentrations of NaCl in the microplastic solution were set to 0.005, 0.01, 0.05, 0.1, and 0.5 mol/L. Other experimental conditions were set in accordance with the conditions described in the 'Adsorption studies' section.

As shown in Figure 3, with the increase in ion concentration, the removal efficiency of PS microplastics decreased from 66.71% to 53.23%, and the adsorption capacity of 3D RGO decreased from 533.68 mg/g to 425.87 mg/g. At pH = 6, 3D RGO was positively charged whereas PS microplastics were negatively charged. The Na^+ in the solution adsorbed to the surface of PS microplastics, which neutralized negative charges on the surface of PS microplastics, thereby weakening the electrostatic attraction between 3D RGO and PS microplastics (Wu *et al.* 2019). Therefore, the adsorption capacity of 3D RGO on PS microplastics decreased.

Adsorption isotherms

To learn about the adsorption mechanism and characteristics of 3D RGO on PS microplastics, different initial concentrations of PS microplastics were set to analyze adsorption isothermal models. A series of microplastic solutions with concentrations of 0.1, 0.2, 0.3, 0.4, 0.5, 0.6, 0.7, and 0.8 g/L was prepared, and the pH of all solutions was adjusted to 6. Other experimental conditions were set in accordance with the conditions described in the 'Adsorption studies' section.

As shown in Figure 4, when the initial concentration (C_0) of the solution increased from 100 mg/L to 600 mg/L, the adsorption capacity of 3D RGO increased from 118.72 mg/g to 533.83 mg/g. The adsorption capacity reached a plateau at higher than 600 mg/L. With the increase in the initial concentration of the solution, the removal efficiency of PS microplastics decreased from 89.04% to 66.73%. The adsorption sites on the surface of 3D RGO are incompletely covered when the initial concentration is low. The probability of collision contact with the adsorption site of the 3D RGO surface increases during the

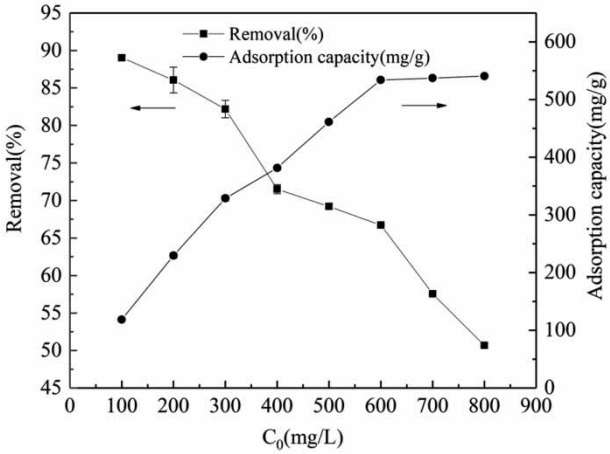

Figure 4 | Effect of different initial concentrations on the adsorption of PS microplastics on 3D RGO.

adsorption process when the initial concentration is high. Thus, the adsorption capacity of the 3D RGO on microplastics is increased. When the initial concentration is higher than 600 mg/L, the adsorption capacity of 3D RGO is unchanged. This finding indicates that the adsorption is saturated. Therefore, 600 mg/L is the optimal initial concentration.

Langmuir and Freundlich models are generally applicable for most adsorptions. The Langmuir adsorption isotherm assumes that adsorption is monolayer and occurs on homogeneous surfaces. In addition, the Freundlich adsorption isotherm can describe adsorption on heterogeneous surfaces, and it is an empirical equation. The corresponding linear formulas are listed as follows:

$$\text{Langmuir adsorption isotherm: } \frac{C_e}{Q_e} = \frac{C_e}{Q_{max}} + \frac{1}{K_L Q_{max}} \quad (5)$$

$$\text{Freundlich adsorption isotherm: } \ln Q_e = \ln K_F + \frac{1}{N} \ln C_e \quad (6)$$

where C_e (mg/L) is the concentration of the microplastic solution at the equilibrium of adsorption; Q_e (mg/g) is the adsorption capacity at the equilibrium of adsorption; Q_{max} (mg/g) is the maximum adsorption capacity per unit mass of the adsorbent; K_L (L/mg) is the Langmuir constant; K_F is the Freundlich constant, indicating the adsorption capacity; N is the Freundlich constant, indicating the adsorption strength.

The Langmuir and Freundlich isotherm plots for the adsorption of PS microplastics on 3D RGO are shown in Figure 5(a) and 5(b), and the calculated values are presented in Table 1. Fitting results showed that the adsorption of PS

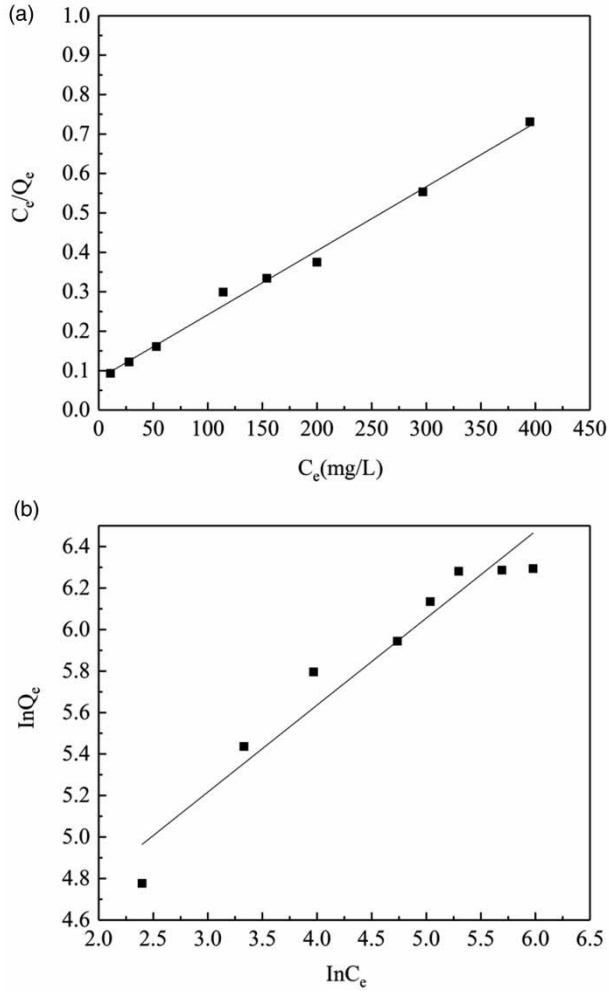

Figure 5 | Adsorption isotherms of 3D RGO. (a) Langmuir adsorption isotherm, (b) Freundlich adsorption isotherm.

microplastics on 3D RGO corresponded to the Langmuir adsorption isotherm model with high correlation coefficient ($R^2 = 0.992$). This finding indicates that the adsorption behavior of 3D RGO for microplastic is monolayer adsorption, and active sites on the surface of 3D RGO are homogeneous. The maximum adsorption capacity obtained from the Langmuir adsorption isotherm model was 617.28 mg/g under the condition of pH = 6 at 26 °C.

Table 1 | Parameters of two adsorption isotherms

	Langmuir adsorption isotherm			Freundlich adsorption isotherm		
Temperature	K_L	Q_{max} (mg/g)	R^2	K_F	1/N	R^2
26 °C	0.02	617.28	0.992	52.46	0.418	0.930

In addition, the dimensionless constant (R_L) can usually be used to evaluate the merits of adsorption performance in the Langmuir adsorption isotherm model (Çolak *et al.* 2009; Mi *et al.* 2012). Its formula is as follows:

$$R_L = \frac{1}{1 + K_L C_0} \tag{7}$$

where K_L (L/mg) is the Langmuir constant; C_0 (mg/L) is the initial concentration of the microplastic solution. As shown in Figure S4 (Supplementary material), R_L is always between 0 and 1 with the increase in the initial concentration, indicating a good adsorption performance for 3D RGO on PS microplastics (Çolak *et al.* 2009).

Adsorption mechanisms

The surface morphology of 3D RGO after adsorption of PS microplastics was analyzed by SEM and XRD, as shown in Figures 6(a)–6(d) and 7. Figure 6(a) and 6(b) show that some PS microplastics were embedded in the pore structure and folds, and some PS microplastics were uniformly and densely distributed on the sheets of the 3D RGO after adsorption. As shown in Figure 6(c) and 6(d), 3D RGO provides rich active sites to adsorb PS microplastics tightly on the surface even at the edge of the 3D RGO. 3D RGO has a large and smooth graphite layer, which produces a π–π effect. It easily adsorbs organic pollutants containing π electrons, forming a stable complex and successfully removing organic pollutants. PS microplastics are macromolecular organics containing π electrons. Charges are uniformly distributed throughout the conjugated system, and their properties are stable. Therefore, the adsorption of PS microplastics on 3D RGO was attributed to the strong π–π interaction between the carbon ring of 3D RGO and the benzene ring of PS microplastics (Chen *et al.* 2011; Pei *et al.* 2013). As shown in Figure 7, 3D RGO showed a broad peak centered at 25°, and PS microplastics exhibited characteristic amorphous diffraction peaks around 20°. Both peaks appeared in the XRD pattern of the 3D RGO after adsorption and had a broadening trend, indicating that PS microplastics adsorbed onto the 3D RGO.

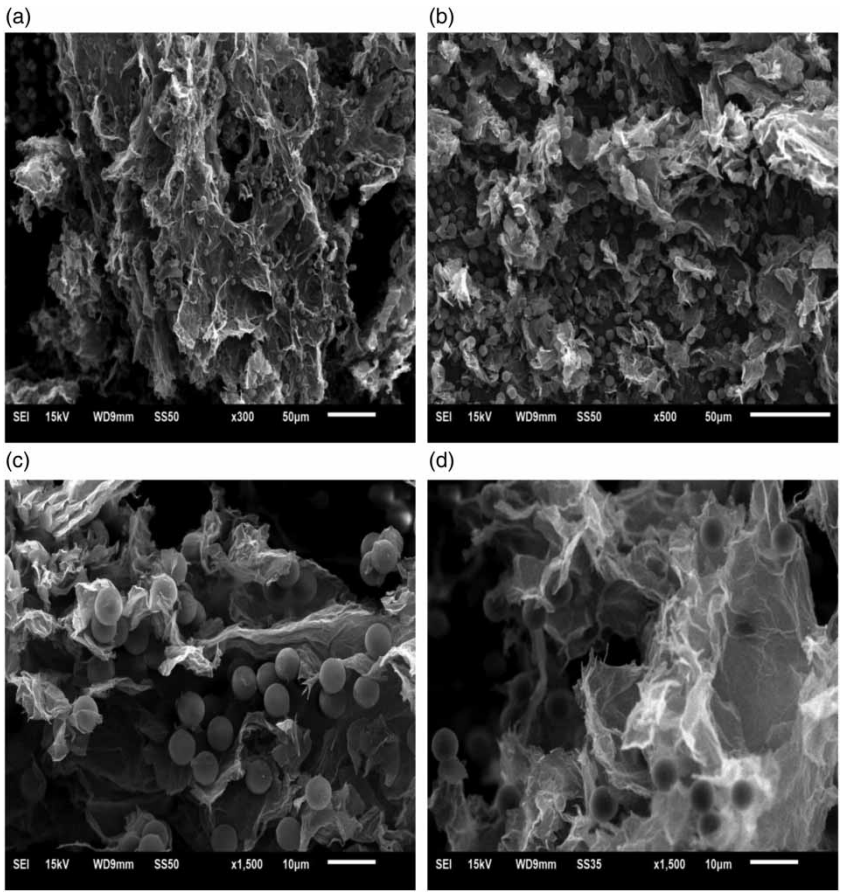

Figure 6 | SEM images of 3D RGO after adsorption, magnified (a) 300 times, (b) 500 times, (c) 1,500 times, and (d) 1,500 times.

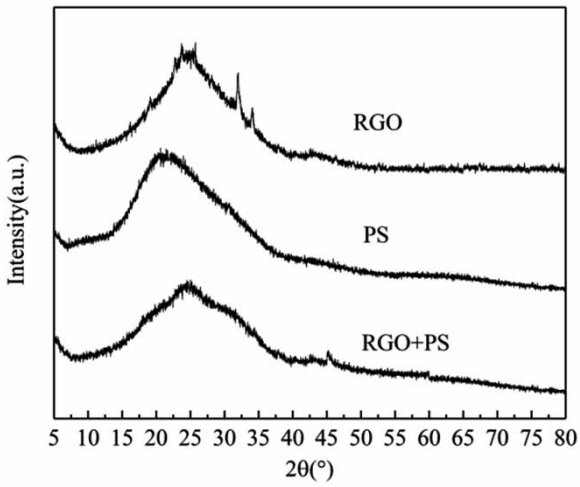

Figure 7 | XRD patterns of 3D RGO, PS microplastics, and 3D RGO after adsorption.

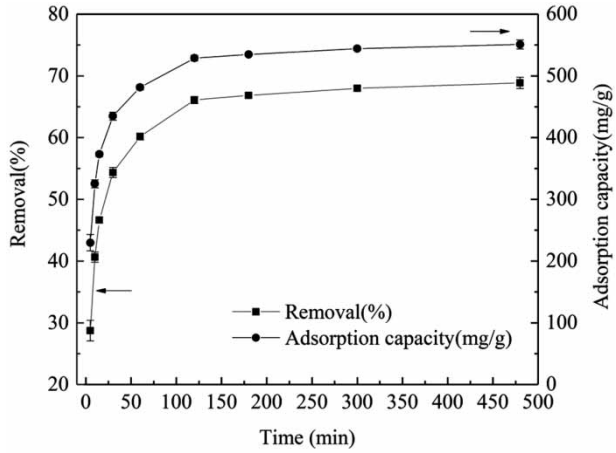

Figure 8 | Effect of different adsorption time on the adsorption of PS microplastics on 3D RGO.

Under the action of oscillation, PS microplastics rapidly migrated from the edge to the surface of the 3D RGO due to electrostatic attraction. The loose pore structure of 3D RGO and the large specific surface area provided a large number of active sites for PS microplastics. The microplastics diffused slowly inside the 3D RGO due to the physical retentive action of the pore structure and the strong π–π force. Therefore, the adsorption of PS microplastics on 3D RGO was mainly attributed to the strong π–π force by using electrostatic attraction and physical retention.

To learn more about the adsorption process of 3D RGO on PS microplastics, a different adsorption time was set to analyze the adsorption kinetic models. The mixture was placed in a water-bathing constant-temperature vibrator and shaken for 5–480 minutes.

As shown in Figure 8, in the first 30 minutes, the removal efficiency of microplastics increased sharply from 28.71% to 54.35%. The removal efficiency of microplastics slowly increased from 54.35% to 66.10% between 30 and 120 minutes. After 120 minutes, the removal efficiency of microplastics and the adsorption capacity of 3D RGO are unchanged. This finding indicates that the adsorption of microplastics on 3D RGO reached equilibrium after 120 minutes.

Two kinetic models are used to fit the adsorption process. The corresponding linear formulas are listed as follows:

$$\text{Pseudo-first-order: } \ln(Q_e - Q_t) = \ln Q_e - K_1 t \tag{8}$$

$$\text{Pseudo-second-order: } \frac{t}{Q_t} = \frac{1}{K_2 Q_e^2} + \frac{t}{Q_e} \tag{9}$$

where t (min) is the contact time; K_1 (min^{-1}) and K_2 [g/(mg·min)] are pseudo-first-order and pseudo-second-order constants, respectively; Q_t and Q_e (mg/g) are the adsorption capacity at t min and adsorption equilibrium, respectively. In addition, H [mg/(g·min)] is the initial rate of adsorption of microplastics on 3D RGO. The corresponding formula is as follows:

$$H = K_2 Q_{e,2}^2 \tag{10}$$

The pseudo-first-order and pseudo-second-order kinetic plots for the adsorption of PS microplastics on 3D RGO are shown in Figure 9(a) and 9(b), and the kinetic parameters, which can be calculated from the plots, are presented in Table 2. Fitting results showed that the adsorption of PS microplastics on 3D RGO fitted well to the pseudo-second-order kinetic model with high correlation coefficient ($R^2 = 0.999$). The calculated adsorption capacity ($Q_{e,cal}$) obtained from the pseudo-second-order kinetic model was 558.66 mg/g, which was close to the experimental adsorption capacity ($Q_{e,exp}$). The influencing factors of the pseudo-second-order kinetic model mainly include the formation of chemical bonds (Freundlich 1906). Therefore, the adsorption of microplastics on 3D RGO is mainly chemical adsorption.

Furthermore, to learn about the migration process of PS microplastics adsorbed onto the surface of 3D RGO, the intraparticle diffusion model was used, the formula of which is as follows:

$$Q_t = K_p t^{0.5} + C \tag{11}$$

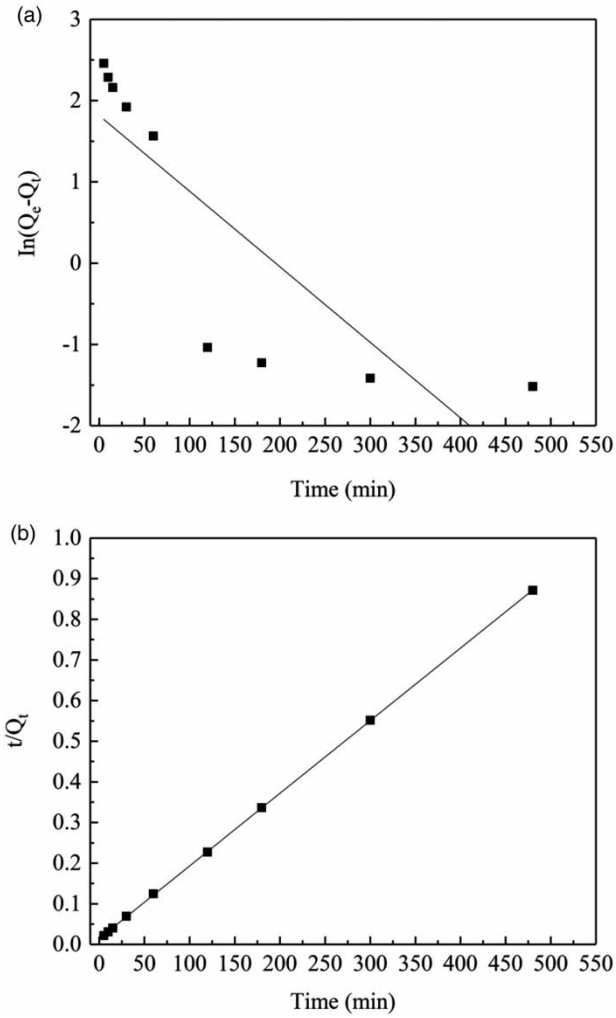

Figure 9 | Adsorption kinetics of 3D RGO. (a) Pseudo-first-order kinetic model, (b) pseudo-second-order kinetic model.

where K_p is the diffusion model constant; t (min) is the adsorption time; C is the constant related to the thickness of the boundary layer; Q_t (mg/g) is the adsorption capacity at t minutes.

The linear plot of Q_t versus $t^{1/2}$ is shown in Figure S5 (Supplementary material). The figure shows that the plot is not a straight line passing through the origin. It is a curve divided into three stages, indicating that intraparticle diffusion is not the only step to control the adsorption process. In the first stage, the slope of the line is large, indicating that the microplastics diffuse rapidly from the edge to the surface of the 3D RGO. In the second stage, the slope of the line is smaller than that of the first stage, indicating that the migration of microplastics into the internal structure of 3D RGO through internal diffusion is a slow adsorption process. In the third stage, the slope of the line tends to be horizontal, indicating that the adsorption of 3D RGO on PS microplastic reaches the adsorption equilibrium. Therefore, the adsorption of microplastics on 3D RGO is mainly accomplished by two stages of membrane diffusion and internal diffusion of particles. In accordance with some reported research (Barghi *et al.* 2014; Fattahi *et al.* 2014), the researchers can also speculate that the factors affecting the mass transfer limitation may include the concentration of PS microplastics in the solution and the distribution and size of the 3D RGO pore. This finding can be further studied separately.

To further learn about the energy changes in the adsorption process, a different adsorption temperature was set to analyze the adsorption thermodynamics.

As shown in Figure 10, with the increase in temperature, the removal efficiency of microplastics increased from 66.83% to 72.63%, and the adsorption capacity of 3D RGO increased from 534.60 mg/g to 580.98 mg/g. This finding indicates that the increase in temperature is good for the adsorption of microplastics on 3D RGO probably because the diffused microplastics inside the 3D RGO are accelerated. However, the temperature was set to 26 °C because the removal efficiency did not change remarkably, and taking energy saving into consideration.

The thermodynamic formulas are as follows:

$$\ln\left(\frac{Q_e}{C_e}\right) = \frac{\Delta S\theta}{R} - \frac{\Delta H\theta}{RT} \tag{12}$$

$$\Delta G\theta = \Delta H\theta - T\Delta S\theta \tag{13}$$

where ΔH^θ (kJ/mol) is the enthalpy change, ΔS^θ (J/(mol·K)) is the entropy change, ΔG^θ (kJ/mol) is the Gibbs free

Table 2 | Parameters of two adsorption kinetics

	Pseudo-first-order			Pseudo-second-order			
$Q_{e,exp}$ (mg/g)	$Q_{e,cal}$ (mg/g)	K_1 (min^{-1})	R^2	$Q_{e,cal}$ (mg/g)	K_2 (g/(mg·min))	R^2	H (mg/(g·min))
528.76	6.15	0.093	0.664	558.66	0.226	0.999	70.472

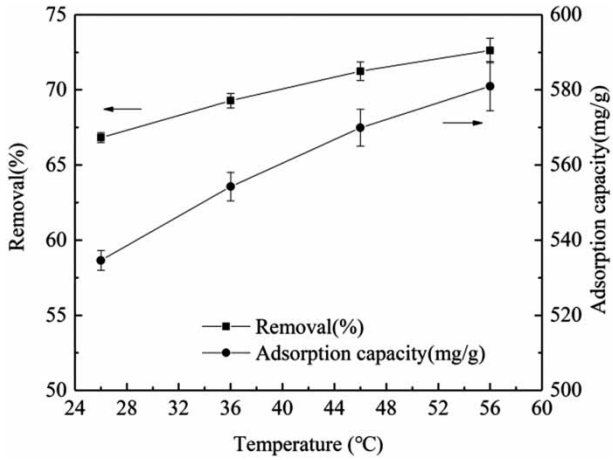

Figure 10 | Effect of different temperatures on the adsorption of microplastics on 3D RGO.

energy change, R/J·(mol·K)$^{-1}$ is the molar gas constant, and T/K is the absolute temperature.

The plot of $\ln(Q_e/C_e)$ versus $1/T$ is presented in Figure 11, and the calculated parameters are shown in Table 3. As shown in Table 3, ΔH^θ is greater than zero, indicating that the adsorption of microplastics is an endothermic process (Tan *et al.* 2009). ΔS^θ is greater than zero, indicating that the chaos in the interface between 3D RGO and microplastics during adsorption is increased (Tan *et al.* 2009). ΔG^θ is always less than zero, indicating that the adsorption process is spontaneous (Çolak *et al.* 2009). Therefore, the adsorption of microplastics on 3D RGO is a spontaneous endothermic process, which may enhance adsorption.

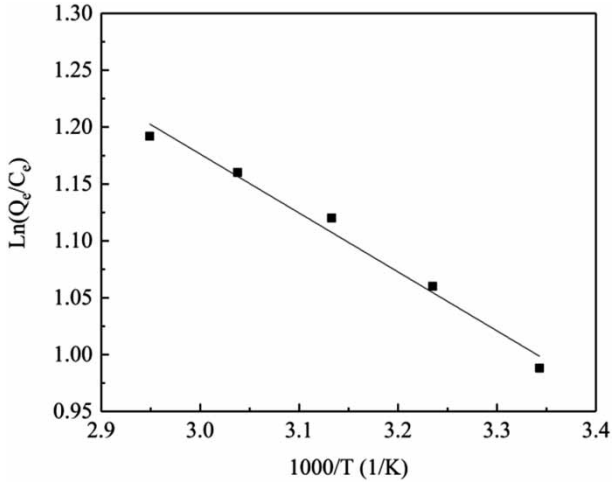

Figure 11 | Plot of $\ln(Q_e/C_e)$ versus $1/T$.

Table 3 | Parameters of adsorption thermodynamics

Temperature/K	ΔH^θ (kJ/mol)	ΔS^θ (J/(mol·K))	ΔG^θ (kJ/mol)
300	7.54	33.5	−2.48
310			−2.81
320			−3.15
330			−3.48

THE ADSORPTION OF PS MICROPLASTICS ON 3D RGO IN ACTUAL WATER SAMPLES

The distilled water used in the experiment was changed for actual water samples to analyze the practical application possibilities of this method. As shown in Figure S6 (Supplementary material), the result shows that the removal efficiency and the adsorption capacity of 3D RGO on PS microplastics in tap water (56.08%, 448.60 mg/g) and micropolluted water (53.85%, 430.78 mg/g) are lower than that of 3D RGO in distilled water (66.63%, 533.06 mg/g). This finding may be due to the multiple effects of metal ions, organic matter, algae secretions, ammonia nitrogen, and other pollutants in the tap water and micropolluted water on the adsorption. For example, metal ions and some pollutants, such as humic acids, are charged under the influence of environmental factors. At the same time, some small suspended particles may block the pore structure of the adsorbent. However, in general, the removal efficiency of 3D RGO on PS microplastics in actual water samples is above 50%, indicating that the utilization of 3D RGO on the adsorption of PS microplastics is effective.

CONCLUSION

Therefore, the researchers have successfully used porous 3D RGO as adsorbent to remove the microscaled PS (PS microplastic) in water. This approach could be regarded as the imitation of PS microplastics in natural water. Under the optimal conditions of pH = 6, $C_0 = 600$ mg/L, $t = 120$ min, and $T = 26\,^\circ$C, the maximum adsorption capacity of 3D RGO on PS microplastics was 617.28 mg/g. The adsorption was mainly based on the strong π–π interaction between graphene and PS microplastics, and the spatial structure of 3D RGO further facilitated the capture of PS microplastics. The result showed that the adsorption by 3D RGO (1.5 mg) of PS microplastic solution (0.6 g/L) reached the adsorption equilibrium after 2 h. The Langmuir adsorption isotherm model and pseudo-second-order kinetic model fitted well with the

experimental data. Moreover, the result of the adsorption thermodynamic analysis showed that the adsorption of PS microplastics was a spontaneous endothermic process. In the practical application for tap water and lake water, this method also exhibited good performance on the PS microplastic removal. Thus, this approach has a promising potential for effective microplastic treatment in the future.

ACKNOWLEDGEMENT

This study was supported by the National Science Foundation of Jiangsu Province (No. BK20180717).

SUPPLEMENTARY MATERIAL

The Supplementary Material for this paper is available online at https://dx.doi.org/10.2166/wst.2020.269.

REFERENCES

Akhtar, J., Amin, N. A. S. & Shahzad, K. 2015 A review on removal of pharmaceuticals from water by adsorption. *Desalination and Water Treatment* **57** (27), 1–19.

Altmann, J., Rehfeld, D., Träder, K., Sperlich, A. & Jekel, M. 2016 Combination of granular activated carbon adsorption and deep-bed filtration as a single advanced wastewater treatment step for organic micropollutant and phosphorus removal. *Water Research* **92**, 131–139.

Auta, H. S., Emenike, C. U. & Fauziah, S. H. 2017 Distribution and importance of microplastics in the marine environment: a review of the sources, fate, effects, and potential solutions. *Environment International* **102** (5), 165–176.

Barghi, B., Fattahi, M. & Khorasheh, F. 2014 The modeling of kinetics and catalyst deactivation in propane dehydrogenation over Pt-Sn/γ-Al_2O_3 in presence of water as an oxygenated additive. *Petroleum Science & Technology* **32** (10), 1139–1149.

Browne, M. A., Dissanayake, A., Galloway, T. S., Lowe, D. M. & Thompson, R. C. 2008 Ingested microscopic plastic translocates to the circulatory system of the mussel, *Mytilus edulis* (L.). *Environmental Science & Technology* **42** (13), 5026–5031.

Carr, S. A., Liu, J. & Tesoro, A. G. 2016 Transport and fate of microplastic particles in wastewater treatment plants. *Water Research* **91**, 174–182.

Chen, D., Li, L. & Guo, L. 2011 An environment-friendly preparation of reduced graphene oxide nanosheets via amino acid. *Nanotechnology* **22** (32), 325601.

Çolak, F., Atar, N. & Olgun, A. 2009 Biosorption of acidic dyes from aqueous solution by *Paenibacillus macerans*: kinetic, thermodynamic and equilibrium studies. *Chemical Engineering Journal* **150** (1), 122–130.

Cole, M., Lindeque, P., Halsband, C. & Galloway, T. S. 2011 Microplastics as contaminants in the marine environment: a review. *Marine Pollution Bulletin* **62** (12), 2588–2597.

Cózar, A., Echevarría, F., González-Gordillo, I. J., Irigoien, X., Ubeda, B., Hernández-León, S., Palma, A. T., Navarro, S., García-de-Lomas, J., Ruiz, A., Fernández-de-Puelles, M. L. & Duarte, C. M. 2014 Plastic debris in the open ocean. *Proceedings of the National Academy of Sciences* **111** (28), 10239–10244.

Farrell, P. & Nelson, K. 2013 Trophic level transfer of microplastic: *Mytilus edulis* (L.) to *Carcinus maenas* (L.). *Environmental Pollution* **177**, 1–3.

Fattahi, M., Kazemeini, M., Khorasheh, F. & Rashidi, A. 2014 Kinetic modeling of oxidative dehydrogenation of propane (ODHP) over a vanadium-graphene catalyst: application of the DOE and ANN methodologies. *Journal of Industrial & Engineering Chemistry* **20** (4), 2236–2247.

Fattahi, M., Kazemeini, M., Khorasheh, F. & Rashidi, A. 2015 Morphological investigations of nanostructured V_2O_5 over graphene used for the ODHP reaction: from synthesis to physiochemical evaluations. *Catalysis Science & Technology* **5**, 910–924.

Freundlich, H. M. F. 1906 Over the adsorption in solution. *Journal of Physical Chemistry* **57**, 385–470.

Ge, X., Shi, L. & Wang, X. 2014 Dechlorination of reformate via chemical adsorption reactions by Ce–Y zeolite. *Industrial & Engineering Chemistry Research* **53** (15), 6351–6357.

Hidalgo-Ruz, V., Gutow, L., Thompson, R. C. & Thiel, M. 2012 Microplastics in the marine environment: a review of the methods used for identification and quantification. *Environmental Science & Technology* **46** (6), 3060–3075.

Huang, F., Zhang, F., Wang, B. & Sun, H. J. 2014 Kinetics and thermodynamics of adsorption of Zn(II) on reduced graphene oxide. *Chinese Journal of Applied Chemistry* **12**, 1458–1464.

Jeong, H. K., Lee, Y. P., Lahaye, R. J. W. E., Park, M. H., An, K. H., Kim, I. J., Yang, C. W., Park, C. Y., Ruoff, R. S. & Lee, Y. H. 2008 Evidence of graphitic AB stacking order of graphite oxides. *Journal of the American Chemical Society* **130** (4), 1362–1366.

Jin, Z., Wang, X., Sun, Y., Ai, Y. & Wang, X. K. 2015 Adsorption of 4-\r, *n*\r, -nonylphenol and bisphenol-a on magnetic reduced graphene oxides: a combined experimental and theoretical studies. *Environmental Science & Technology* **49** (15), 9168–9175.

Kazemeini, M., Nikkhah, M., Fattahi, M. & Vafajoo, L. 2016 Physicochemical properties and catalytic performances of nanostructured V_2O_5 over TiO_2 and γ-Al_2O_3 for oxidative dehydrogenation of propane. *Chemical & Biochemical Engineering Quarterly* **30** (1), 9–18.

Ma, B. W., Xue, W. J., Ding, Y. Y., Hu, C. Z., Liu, H. J. & Qu, J. H. 2019 Removal characteristics of microplastics by Fe-based coagulants during drinking water treatment. *Journal of Environmental Sciences* **78** (4), 267–275.

Magnusson, K. & Fredrik, N. 2014 Screening of microplastic particles in and down-stream a wastewater treatment plant. *Swedish Environmental Research Institute* **55**, 1–22.

Marcano, D. C., Kosynkin, D. V., Berlin, J. M., Sinitskii, A., Sun, Z. Z, Slesarev, A., Alemany, L. B., Lu, W. & Tour, J. M. 2010 Improved synthesis of graphene oxide. *ACS Nano* **4** (8), 4806–4814.

Mi, X., Huang, G., Xie, W., Wang, W., Liu, Y. & Gao, J. 2012 Preparation of graphene oxide aerogel and its adsorption for Cu^{2+} ions. *Carbon* **50** (13), 4856–4864.

Murphy, F., Ewins, C., Carbonnier, F. & Quinn, B. 2016 Wastewater treatment works (wwtw) as a source of microplastics in the aquatic environment. *Environmental Science & Technology* **50** (11), 5800–5808.

Nardecchia, S., Carriazo, D., Ferrer, M. L., Gutiérreza, M. C. & Monte, F. D. 2013 Three dimensional macroporous architectures and aerogels built of carbon nanotubes and/or graphene: synthesis and applications. *Chemical Society Reviews* **42**, 794–830.

Paul-Pont, I., Lacroix, C., Gonzalez Fernandez, C., Hégaret, H., Lambert, C., Le Goïc, N., Frère, L., Cassone, A. L., Sussarellu, R., Fabioux, C., Guyomarch, J., Albentosa, M., Huvet, A. & Soudant, P. 2016 Exposure of marine mussels *Mytilus* spp. to polystyrene microplastics: toxicity and influence on fluoranthene bioaccumulation. *Environmental Pollution* **216** (9), 724–737.

Payan, A., Fattahi, M. & Roozbehani, B. 2018 Synthesis, characterization and evaluations of TiO_2 nanostructures prepared from different titania precursors for photocatalytic degradation of 4-chlorophenol in aqueous solution. *Journal of Environmental Health Science & Engineering* **16** (1), 41–54.

Pei, Z., Li, L., Sun, L., Zhang, S. Z., Shan, X. Q., Yang, S. & Wen, B. 2013 Adsorption characteristics of 1,2,4-trichlorobenzene, 2,4,6-trichlorophenol, 2-naphthol and naphthalene on graphene and graphene oxide. *Carbon* **51**, 156–163.

Pellini, G., Gomiero, A., Fortibuoni, T., Ferrà, C., Grati, F., Tassetti, A. N., Polidori, P., Fabi, G. & Scarcella, G. 2018 Characterization of microplastic litter in the gastrointestinal tract of *Solea solea* from the Adriatic Sea. *Environmental Pollution* **234**, 943–952.

Peng, J., Wang, J. & Cai, L. 2017 Current understanding of microplastics in the environment: occurrence, fate, risks, and what we should do. *Integrated Environmental Assessment & Management* **13** (3), 476–482.

Shen, Y., Fang, Q. & Chen, B. 2015 Environmental applications of three-dimensional graphene-based macrostructures: adsorption, transformation, and detection. *Environmental Science & Technology* **49** (1), 67–84.

Shim, W. J. & Thomposon, R. C. 2015 Microplastics in the ocean. *Archives of Environmental Contamination & Toxicology* **69** (3), 265–268.

Shojaie, A., Fattahi, M., Jorfi, S. & Ghasemi, B. 2018 Synthesis and evaluations of Fe_3O_4-TiO_2-Ag nanocomposites for photocatalytic degradation of 4-chlorophenol (4-CP): effect of Ag and Fe compositions. *International Journal of Industrial Chemistry* **9**, 141–151.

Tajizadegan, H., Torabi, O., Heidary, A. & Golabgir, M. H. 2016 Study of methyl orange adsorption properties on ZnO-Al_2O_3 nanocomposite adsorbent particles. *Desalination & Water Treatment* **57** (26), 12324–12334.

Tan, I. A. W., Ahmad, A. L. & Hameed, B. H. 2009 Adsorption isotherms, kinetics, thermodynamics and desorption studies of 2,4,6-trichlorophenol on oil palm empty fruit bunch-based activated carbon. *Journal of Hazardous Materials* **164** (2–3), 473–482.

Vadahanambi, S., Lee S, H., Kim W, J. & Oh, I. K. 2013 Arsenic removal from contaminated water using three-dimensional graphene-carbon nanotube-iron oxide nanostructures. *Environmental Science & Technology* **47** (18), 10510–10517.

Wardrop, D., Bott, C., Criddle, C., Hale, R., McDevitt, J., Morse, M. & Rochman, C. 2016 *Technical Review of Microbeads/ Microplastics in the Chesapeake Bay*. STAC Publication Number 16-002, Edgewater, MD, USA, p. 27.

Wu, W. M., Yang, J. & Criddle, C. S. 2017 Microplastics pollution and reduction strategies. *Frontiers of Environmental Science & Engineering* **11** (1), 6.1–6.4.

Wu, J., Jiang, R., Lin, W. & Ouyang, G. F. 2019 Effect of salinity and humic acid on the aggregation and toxicity of polystyrene nanoplastics with different functional groups and charges. *Environmental Pollution* **245** (2), 836–843.

Xu, J., Wang, L. & Zhu, Y. 2012 Decontamination of bisphenol a from aqueous solution by graphene adsorption. *Langmuir* **28** (22), 8418–8425.

Yang S, T., Chang, Y., Wang, H., Liu, G. B., Chen, S., Wang, Y. W., Liu, Y. F. & Cao, A. N. 2010 Folding/aggregation of graphene oxide and its application in Cu^{2+} removal. *Journal of Colloid & Interface Science* **351** (1), 122–127.

Zhou, M., Zhai, Y. & Dong, S. 2009 Electrochemical sensing and biosensing platform based on chemically reduced graphene oxide. *Analytical Chemistry* **81** (14), 5603–5613.

First received 14 November 2019; accepted in revised form 27 May 2020. Available online 8 June 2020